Int. J. Nanosci. Nanotechnol., Vol. 7, No. 2, Jun. 2011, pp. 57-64

Synthesis of Three-Layered Magnetic Based Nanostructure for Clinical Application

M. E. Khosroshahi*, L. Ghazanfari

Laser and Nanobiophotonic Lab., Biomaterials Group, Faculty of Biomed. Eng.,
Amir Kabir University of Technology, Tehran, I.R. Iran

(*) Corresponding author: khosro@aut.ac.ir
(Received: 10 May 2011 and Accepted: 25 May 2011)

Abstract:
The main objective of this research was to synthesize and characterize gold-coated Fe_3O_4/SiO_2 nanoshells for clinical applications. Magnetite nanoparticles (NPs) were prepared via co-precipitation. The results showed that smaller particles can be synthesized by decreasing the NaOH concentration, which in our case this corresponded to 35 nm by using 0.9 M of NaOH at 750 rpm. The NPs were then modified with a thin layer of silica using Stober method. The surface of Fe_3O_4/SiO_2 nanoshells was then terminated with amine groups with 3-aminopropyltriethoxysilane (APTS) in ethanol. Small gold colloid (1-3 nm) were adsorbed on the particle surface via the interaction between the negative charge on the Au nanoparticles and the positive charge of $-NH_3$ on the SiO_2 shell modified by APTS. Gold nanoshell formation, morphology and dimensions were assessed with a UV-Vis spectrophotometer, atomic force microscope (AFM), and transmission electron microscope (TEM). The synthesized nanostructures exhibited an absorption peak at ~550 nm with a magnetization value of 1.3 emu/g. Based on the X-ray diffraction (XRD) results, three main peaks of Au were identified. The formation of each layer of a nanoshell is also demonstrated by Fourier transform infrared (FTIR) results.
Keywords: *Multilayer nanostructure; Magnetic properties; UV-vis spectroscopy.*

1. INTRODUCTION

Iron oxide nanoparticles have attracted much interest for biomedical applications due to their outstanding properties including superparamagnetism and low toxicity. In particular, solutions of maghemite (γ-Fe_2O_3) or magnetite (Fe_3O_4) particles in diameter of 7.5-100 nm have shown promise as magnetic fluids for targeted drug delivery. Their potential applications cover various fields especially in biomedical applications [1-3]. For in vivo applications, the magnetic nanoparticles (MNPs) can be coated with a biocompatible and diamagnetic material (such as organic polymers or silica shells [4-6]) to prevent the formation of large aggregates of MNPs and to facilitate functions such as the attachment of drugs. However, to kill the cancer cells or cure the affected tissues by photothermal therapy, the silica coated MNPs need to be coated with particles that have an excellent heat generating ability under controllable conditions. Gold nanoshells exhibit strong absorbance with tunable wavelength in the near-infrared (NIR) region of the electromagnetic spectrum. Not only can these particles be used in biomedical imaging applications, but more importantly, they are potential candidates for localized photothermal therapy because they mediate strong plasmon-induced surface heat flux upon absorption of NIR

light [7-9]. The main objective of this research was to synthesize and characterize magnetite-silica core and gold nanoshells for clinical application such as laser hyperthermia based on surface plasmon resonance effect.

2. EXPERIMENTAL

2.1. Materials

All of analytic reagents were purchased from the indicated suppliers and used without further purification: ferric chloride hexahydrate ($FeCl_3$•$6H_2O$) (99%), ferrous chloride tetrahydrate ($FeCl_2$•$4H_2O$) (99%), sodium hydroxide (NaOH, 99%), hydrochloric acid (HCl, 37%), trisodium citrate (TSC), absolute ethanol, ammonia aqueous (25wt%), $Si(OC_2H_5)_4$ (tetraethyl orthosilicate, TEOS) were purchased from Merck. 3-amino-propyltriethoxysilane (APTS), tetrakis (hydroxymethyl) phosphonium chloride (THPC), chloroauric acid ($HAuCl_4$), potassium carbonate (K_2CO_3), and formaldehyde (37%) were obtained from Sigma-Aldrich (St. Louis, MO). Milli-Q water (specific conductance 0.1 μs/cm) was deoxygenated by bubbling N_2 gas for 1 h prior to the use.

2.2. Instruments

TEM was performed using a Phillips CM-200-FEG microscope operating at 120 kV. Magnetization measurements were carried at 300 K in a magnetic field (H) of up to 10 KOe with a vibrating sample magnetometer (VSM-PAR 155) that can measure magnetic moments as low as 10^{-3} emu. For the magnetization measurements, uncoated dry powders of Fe_3O_4 NPs were obtained by evaporating the water from the solution. XRD measurements were performed at room temperature using a FK60-04 X-ray diffractometer with Cu radiation. FTIR spectra of powders were recorded by EQUINOX 55 FTIR spectrometer. A Dual-scope/ Rasterscope system (C26, DME, Denmark) was used for all imaging by SPM. The microscope was equipped with a scanner that had a maximum XY scan range of 50 by 50μm and a Z range of 3μm and was operated by means of a Scan Master (95-50E), a real-time closed-loop scanning control system that allows for the accurate measurement, repositioning, and zooming in on selected features. Ultraviolet visible spectroscopy (UV−Vis) of the samples was performed with a Lambda 950 spectrophotometer (Perkin-Elmer, USA) from 200 to 1000 nm wavelength.

2.3. Method

An iron oxide dispersion was prepared based on the co-precipitation of $FeCl_2$ and $FeCl_3$ upon addition of aqueous NaOH solution to a mixture of the iron salts at room temperature. Stock solutions of 0.9-1.5 M NaOH were prepared as the alkali sources and the synthesized Fe_3O_4 samples were classified as S1-S4 [10]. The obtained black dispersion was treated with an excess of trisodium citrate solution to give stabilized magnetite NPs. The coating of citrate-modified Fe_3O_4 with silica were carried out in a basic ethanol/water mixture at room temperature [11] using the obtained magnetite dispersion (only sample S1 as an optimized one) as seeds, in which silica is formed by in-situ method through the hydrolysis and condensation of tetraethylorthosilicate (TEOS) at room temperature. Gold seeds were prepared based on Baiker's method [12]. The modified silica NPs with amino terminal functional group were then slowly added into the gold seed solution under stirring. The NPs suspension was subsequently added to a gold growth solution, containing potassium carbonate, aqueous tetrachloroaurate solution, and water. Formaldehyde was then added dropwise to the mixture. When the color of the suspension changed from pale to purple, the suspension was centrifuged and the excess gold NPs with pale-purple color were removed.

3. RESULTS AND DISCUSSION

The size, structure, and chemical composition of the NPs were determined. The mean particle size was examined by TEM imaging (Figure 1). As it is seen in this figure, particle size decreases at lower NaOH%, which in our case, corresponds to 35 nm at 0.9 M of NaOH (Figure 2).

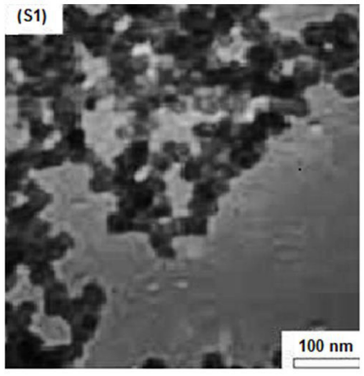

Figure 1: *TEM Micrograph of Fe_3O_4 NPs.*

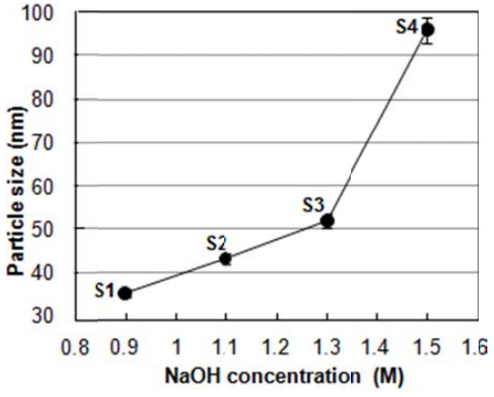

Figure 2: *NaOH concentration vs particle size for unccoated Fe_3O_4 NPs.*

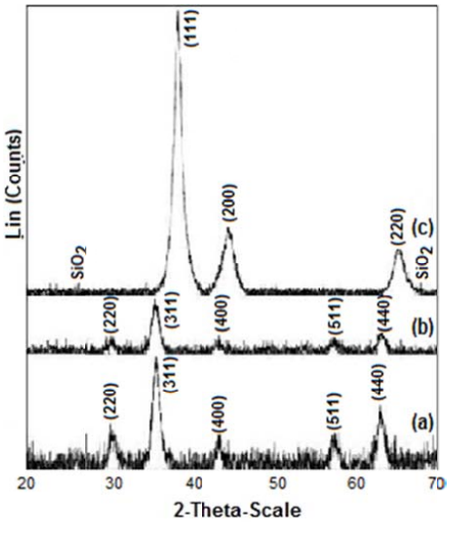

Figure 3: *X-ray diffraction patterns for: (a) citrate-modified Fe_3O_4 NPs, (b) Fe_3O_4/SiO_2 nanoshells, (c) Fe_3O_4/SiO_2/Au nanostructures.*

Figure 3 shows the XRD patterns for (a) citrate-modified Fe_3O_4 NPs, (b) Fe_3O_4 /SiO_2 nanoshells, (c) Fe_3O_4 /SiO_2 /Au nanostructures with each pattern normalized to its maximum intensity. The peaks are indexed with the fcc structure corresponding to magnetite phase. The average size of the crystals was estimated using Scherrer's formula:

$$D_{hkl} = \frac{k\lambda}{\sqrt{B_M^2 - B_S^2 \cos\theta_{hkl}}} \qquad (1)$$

where k is the shape factor, λ the x-ray wavelength, B_M the half maximum line width (FWHM) in radians, B_S the half maximum line width of the instrument, θ the Bragg angle and D_{hkl} the mean size of the ordered (crystalline) domains. The dimensionless shape factor has a typical value of about 0.9, but varies with the actual shape of the crystallite. The XRD results showed that the citrate-modified Fe_3O_4 NPs are about 8 nm. As it can be seen from figure 3b the pattern of silica-coated magnetite displayed the same lines as uncoated magnetite. This indicates that the coated silica is in an amorphous form before it was mixed with the gold solution. However, it appears that the coating of Au particles on silica could induce small crystallization of silica even at room temperature. For the Fe_3O_4/SiO_2/Au nano-structures, the XRD pattern shown in Figure 3c displays three wide peaks that can be identified as the (111), (200), and (220) reflection lines of the Au fcc-cubic phase, indicating the gold particles crystallinity. Considering the fact that most of SiO_2-coated particles are spherical and that usually spherical SiO_2 particles are in the amorphous form, one can deduce that most of the silica nanoshells are in the amorphous phase. Interestingly, the Fe_3O_4 peaks (Figure 3a, b) appearing in the patterns of the SiO_2-coated and citrate-modified Fe_3O_4 NPs are not seen in the pattern of the Au/SiO_2 coated particles shown in Figure 3c. This occurrence can be explained by the strong absorption of and scattering from the Au-coated particles.

The FTIR spectra of NPs in Figure 4a, illustrates the main absorption peaks around 591 and 3422 cm^{-1} corresponding to Fe–O and O–H stretching

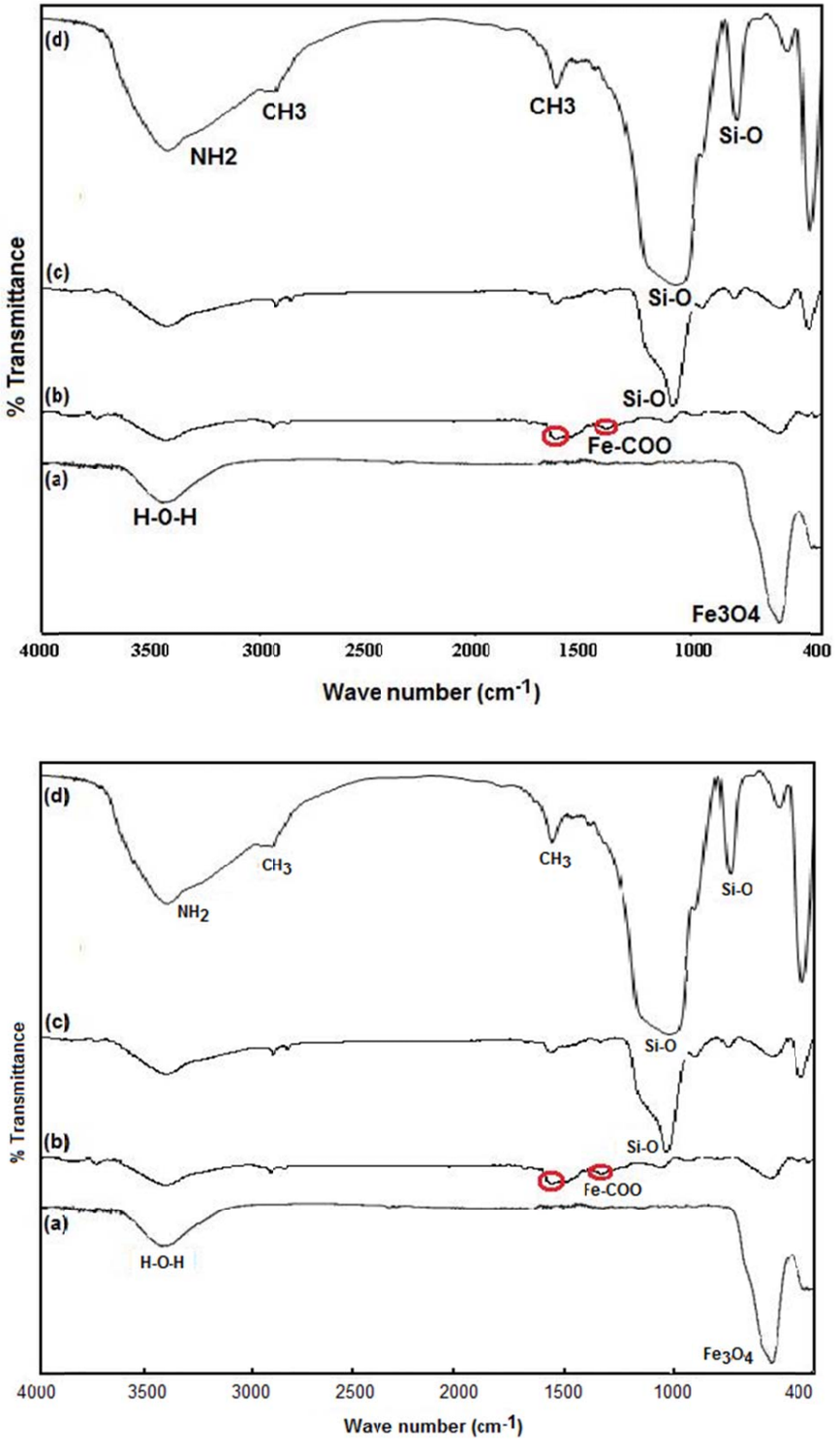

Figure 4: *FT-IR spectra of: (a) uncoated Fe_3O_4 NPs, (b) citrate-modified Fe_3O_4 NPs, (c) Fe_3O_4/SiO_2 nanoshells, (d) Fe_3O_4/SiO_2/APTS nanocomposites.*

vibration modes, respectively. Also, the new absorption peaks observed at 1614 and 1391 cm^{-1} are characteristics of the carboxylate bonds. The presence of magnetite is evident at 418 and 462 cm^{-1}. The absorption peaks of citrate-modified samples at 1622 cm^{-1} and 1397 cm^{-1} are due to the COO–Fe bond, (Figure 4b). The band at 1092 cm^{-1} and 802 cm^{-1} are characteristic peaks of the symmetrical and asymmetrical vibrations of Si–O–Si .The band at 466 cm^{-1} is an indication of the presence of Si–O–Fe (Figure 4c). Figure 4d is the IR spectra of Fe_3O_4 /SiO_2 /APTS nanocomposites. The broad bands near 1092 cm^{-1} and 798 cm^{-1} are the contribution of Si—O. The absorption bands in 2930 and 2850 cm^{-1} are due to stretching vibration of —CH_2. Bands near 3430 and 1633 cm^{-1} exhibit the existence of —NH_2.

Saturation magnetization, M_s, is the main magnetic parameter that has to be characterized when considering the magnetism of a magnetic material. The value of M_s for these particles, was measured about 82 emu/g which steadily increased by increasing their size (Figure 5). It can be seen that the M_s of Fe_3O_4 NPs are close to the bulk value of magnetite which is about 85-100 emu/g. In our case, the M_s value for S1 is slightly higher than the one reported by Yang *et al.* [11].

The SiO_2 /Au shell allows each Fe_3O_4 particle to behave independently, and inter-particle interactions are therefore not important. Figure 6 shows the magnetization curve of the Fe_3O_4 /SiO_2 /Au nanostructures obtained at room temperature using a VSM. The hysteresis loop for the Fe_3O_4 /SiO_2 /Au nanostructures was almost completely reversible, implying that the magnetization curve exhibits zero remanence and coercivity, hence proving that SiO_2 /Au coated Fe_3O_4 NPs have superparamagnetic properties. Thus, these nanocomposites are able to respond to an external magnetic field (1000 Oe) without any permanent magnetization.

The optical absorption (UV-Vis) spectrum of Fe_3O_4 /SiO_2 /Au nanostructures given in Figure 7 is relatively broad compared with that of pure gold colloid where its absorption peak occurs at 520 nm [13]. In addition, the plasmon line-width is dominated by electron surface scattering. The

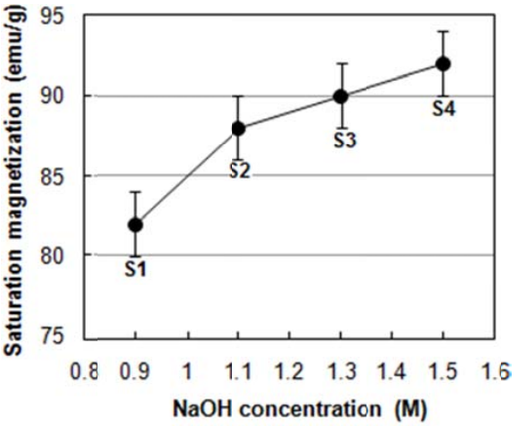

Figure 5: *Variation of saturation magnetization with particle size for uncoated Fe_3O_4 NPs.*

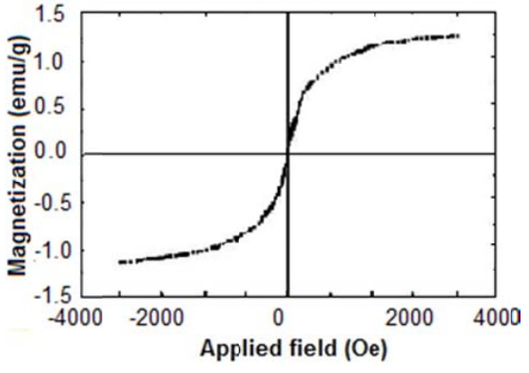

Figure 6: *Variation of Fe_3O_4/SiO_2/Au nanostructures magnetization with applied field.*

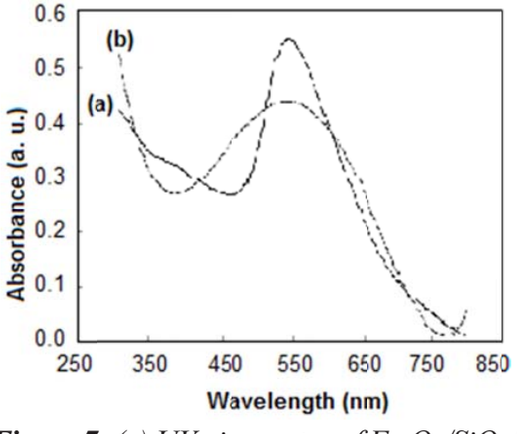

Figure 7: *(a) UV-vis spectra of Fe_3O_4/SiO_2/Au nanostructures- (b) represents fourth- order polynomial $y=2E-10x^4-5E-07x^3+0.130x$ $=16.61$, $R^2=0.865$.*

nanostructures with optical plasmon resonance peaks in 500-600 nm regions, can be used as a powerful tool in bio-imaging and bio-sensing applications. According to Mie's theory [14], the broadening of resonance absorption is related to the size, shape, and aggregation of the gold nanoshells. When gold particles aggregate on the surface of amino-modified silica, the peak plasmon resonance wavelength will be shifted to the near-infrared range. Furthermore, the silica layer provides a dielectric interface for red-shifting the plasma resonance in electromagnetic spectrum resulting from the charge variation of the gold NPs within the core/shell structure. In Figure 7, the intensity maximum of the absorption peaks is plotted against the wavelength. It is obvious that, the absorption peak decrease nonlinearly. The dashed line represents fourth-order polynomial Abs = $2\times10^{-10}x^4$ - $5\times10^{-7}x^3$ - 0.13x + 16.61 (R^2=0.865) fits to the points, which was determined from the calculated absorption spectrum.

The scattering (σ_{sca}), extinction (σ_{ext}), and absorption (σ_{abs}) cross sections of a nanoshell can be calculated according to the Mie theory:

$$\sigma_{sca} = \left(\frac{N_T \lambda^2}{2\pi}\right) \sum_{n=1}^{\infty} (2n+1)(|a_n|^2 + |b_n|^2) \quad (2)$$

$$\sigma_{ext} = \left(\frac{N_T \lambda^2}{2\pi}\right) \sum_{n=1}^{\infty} (2n+1)\, Re\{|a_n|^2 + |b_n|^2\} \quad (3)$$

$$\sigma_{abs} = \sigma_{ext} - \sigma_{sca} \quad (4)$$

Where N_T is the number of NPs, λ is the wavelength of incident radiation, and a_n and b_n are the scattering coefficients.

TEM images were used to observe the agglomeration state, particle size distribution, and morphology of Fe_3O_4/SiO_2/Au nanoshells. At first, the silica layer can stabilize the magnetic particles by bringing negative charges on the surface of shell that enhance the coulomb repulsion of the magnetic particles and by sheltering the magnetic dipole interaction, respectively. When NPs of multiple sizes were present, ordered regions with larger NPs in the center and smaller NPs at the edges were formed. The TEM image shows the clusters of small gold NPs are assembled on the surfaces of larger silica NPs. With very few exceptions, most previously observed self-assembled structures involve hundreds or thousands of NPs and long-range ordering. Amine-functionalized silica NPs (treated with APTS) exhibited heavy coverage of gold NPs as shown in Figure 7 which is comparable to that reported by Westcott et al. [15].

TEM is still the most commonly used microscopy technique for visualizing colloidal particles, though atomic force microscopy (AFM) is also a serious alternative which provides more information about particles. The typical AFM forces are mechanical contact force, Van der Waals force, capillary forces, electrostatic forces, magnetic force (MFM) etc. Individual particles, size information (length, width, and height) and other physical properties (such as morphology and surface texture) are measured by AFM. AFM relies on the interaction between the specimen and a nanometric tip attached to a cantilever, which scans the sample surface. The force constants were 0.1 N/m for contact-mode imaging. AFM images of nanoshells shown in Figure 9, is expected to exhibit considerable surface roughness due to the agglomeration of the nanoshells which in our case it was 618 pm. In addition, the agglomeration of NPs is evident in the topography image because the powders were confined directly on the copper tape. Both height and phase images are useful for visualizing the morphology and size of the Fe_3O_4/SiO_2/Au nanostructures, but the cluster composition is better seen by the phase image mode. Clusters of few particles are mainly formed during drying due to the capillary forces even when highly diluted samples were used.

4. CONCLUSION

In conclusion, we have presented a controlled coprecipitation method, which demonstrates the feasibility of synthesizing of magnetite NPs with least diameter value of 35nm and good magnetic

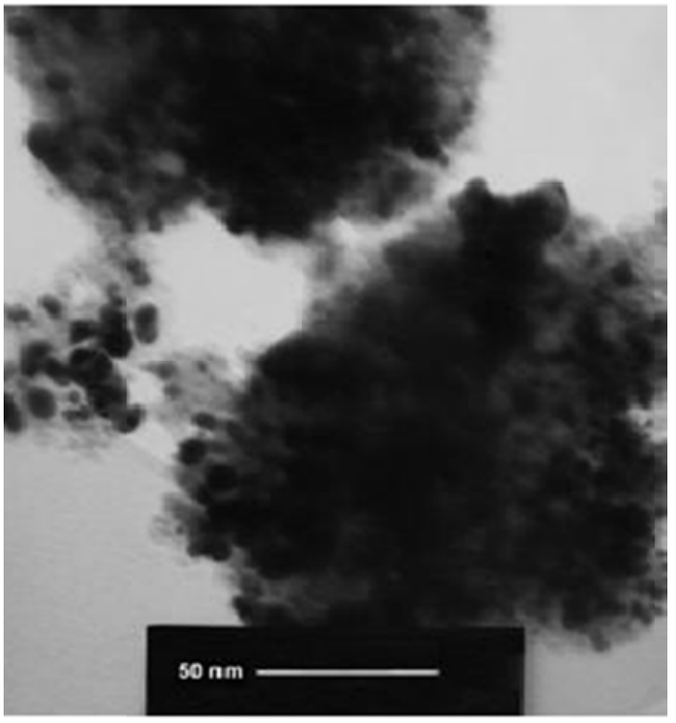

Figure 8: *TEM micrograph of $Fe_3O_4/SiO_2/Au$ nanostructures.*

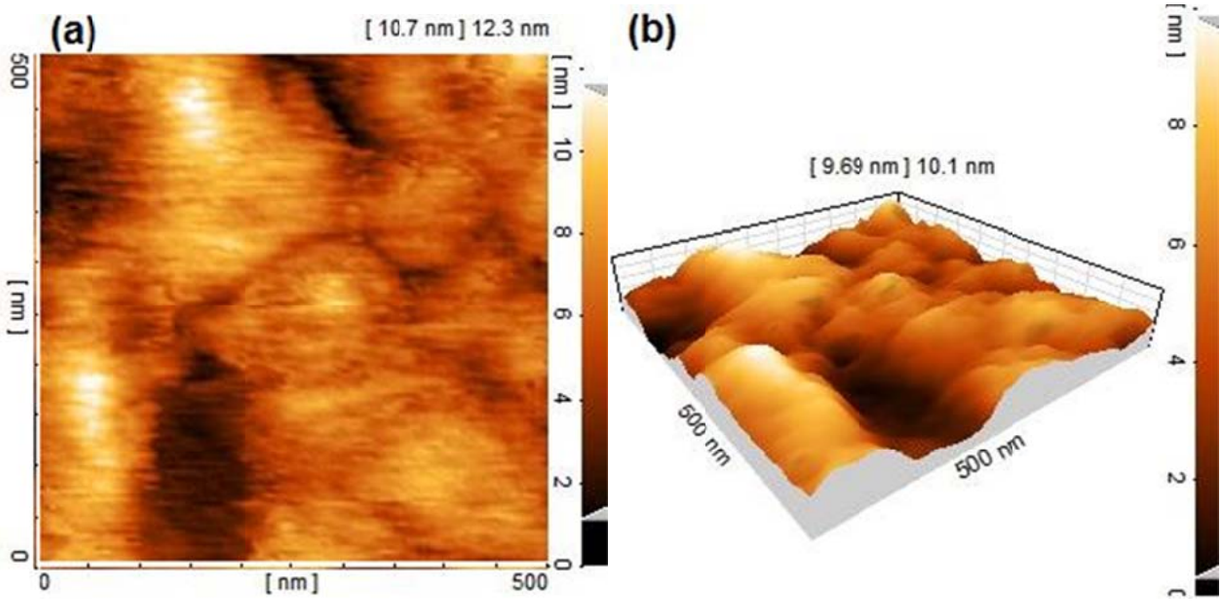

Figure 9: *AFM micrographs of $Fe_3O_4/SiO_2/Au$ nanostructures in (a) 2D and (b) 3D-height mode.*

properties using 0.9M of NaOH. For uncoated Fe_3O_4 NPs, the results showed an octahedral geometry with saturation magnetization range of (80-100) emu/g for particles between (35-96) nm. The diameter of Fe_3O_4/SiO_2 nanocomposites synthesized by Stober method was 50 nm. The final gold nanoshells synthesized by Baiker method with 85 nm as particle size, demonstrated a magnetization value of 1.3 emu/g. UV-Vis spectroscopy demonstrated an absorption spectrum between 500-600 nm. The results provide us with a better understanding of the structural, magnetic and optical properties for gold and silica doubly coated Fe_3O_4 NPs. The resulting multifunctional nanoshells combine the attractive photothermal properties of gold nanoshells with the magnetic properties of Fe_3O_4 NPs which can be used for targeting purpose. Combining the advances in biophotonics and nanotechnology can offer an opportunity to significantly impact future strategies towards the diagnosis and therapy of cancer.

REFERENCES

1. H.Y. Park, M.J. Schadt, L.Y. Wang, I.I.S. Lim, P.N. Njoki, S.H. Kim, M.Y. Jang, J. Luo, C.J.Zhong, Langmuir 23 (2007) 9050.
2. M.E. Khosroshahi, M. Tahriri, M. Mahmoodi, 1st Asian Biomaterials Congress, Tsukuba, Japan, December 2007.
3. S. Kayal, R.V. Ramanujan, Mat. Sci. Eng. C 30 (2010) 484.
4. Y.H. Deng, C.C. Wang, J.H. Hu, W.L. Yang, Sh.K. Fu, Colloids and Surfaces A: Physicochem. Eng. Aspects 262 (2005) 87.
5. Y. Kobayashi, S. Saeki, M. Yoshida, D. Nagao, M. Konno, J. Sol-Gel Sci. Tech. 45 (2008) 35.
6. M. E. Khosroshahi, L. Ghazanfari, Physica E 42 (2010) 1824.
7. X. Ji, R. Shao, A.M. Elliott, R.J. Stafford, E. Esparza-Coss, J.A. Bankson, G. Liang, Z. Luo, K. Park, J. T. Markert, C. Li, J. Phys. Chem. C 111 (2007) 6245.
8. K. Park, G. Liang, X. Ji, Z.P. Luo, C. Li, M.C. Croft, J.T. Markert, J. Phys. Chem. C 111 (2007) 18512.
9. C. Fang, K. Qian, J. Zhu, S. Wang, X. Lv, S. Yu, Nanotech. 19 (2008) 125601.
10. Y. H. Deng, C.C. Wang, J.H. Hu, W.L. Yang, S. K. Fu, Colloid and surfaces A: Physiochem. Eng. Aspects 262 (2005) 87.
11. D. Yang, J. Hu, S. Fu, J. Phys. Chem. C 113 (2009) 7646.
12. T. Pham, J.B. Jackson, N.J. Halas, T.R. Lee, Langmuir 18 (2002) 4915.
13. L. L. Pang, J.S. Li, J.H. Jiang, Y. Le, G.L. Shen, R.Q. Yu, Sensors and Actuators B, 127 (2007) 311.
14. S. M. Scholz, R. Vacassy, J. Dutta, H. Hofmann, J. Appl. Phys. 83 (1998) 7860.
15. S. L. Westcott, S. J. Oldenburg, T.R. Lee, N.J. Halas, Langmuir 14 (1998) 5396.